Electronic Supplementary Material (ESI) for Nanoscale.
This journal is © The Royal Society of Chemistry 2020

Supporting Information

Arbitrary deformable and high-strength electroactive polymer/ MXene anti-exfoliative composite films assembled into high performance flexible all-solid-state supercapacitors

Yang Zhou,† Yubo Zou,† Zhiyuan Peng,† Chuying Yu,† Wenbin Zhong,†,*

† College of Materials Science and Engineering, Hunan University, Changsha, 410082, P. R. China.

*E-mail address: wbzhong@hnu.edu.cn (W. Zhong)

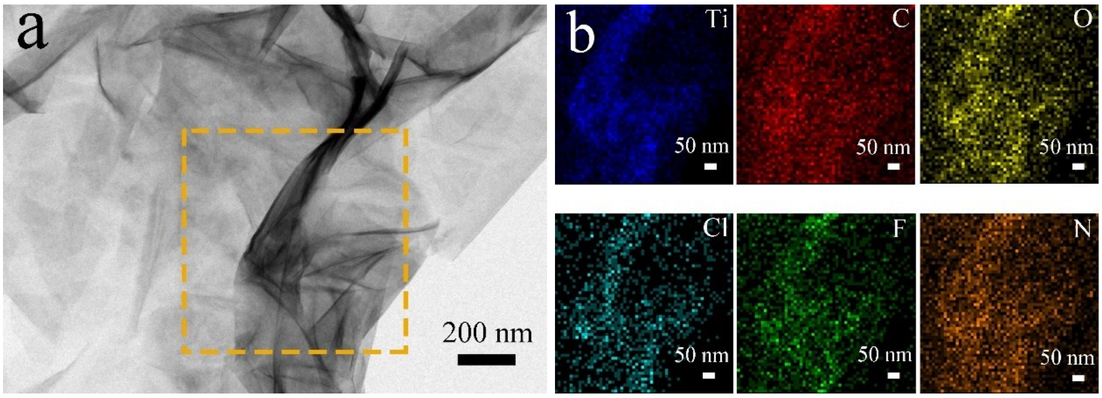

Fig. S1 (a) STEM image and (b) Elemental mapping images of i-PANI@$Ti_3C_2T_x$.

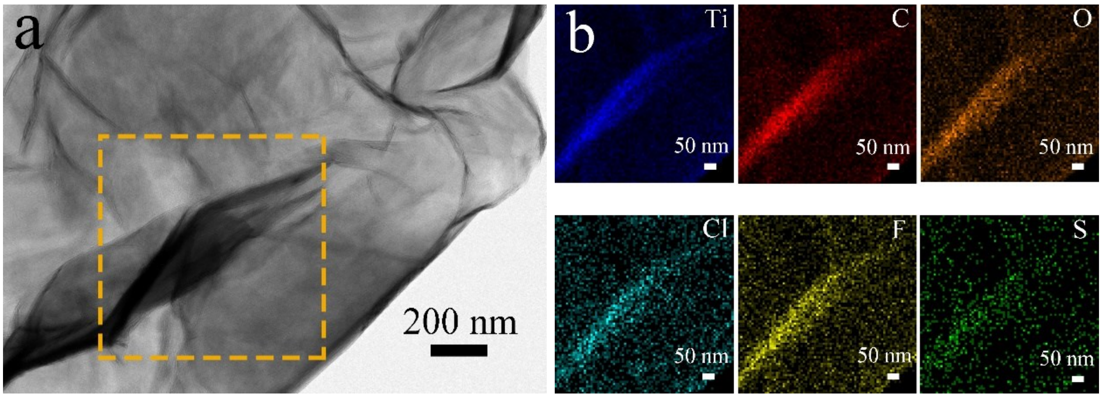

Fig. S2 (a) STEM image and (b) Elemental mapping images of Lig@$Ti_3C_2T_x$.

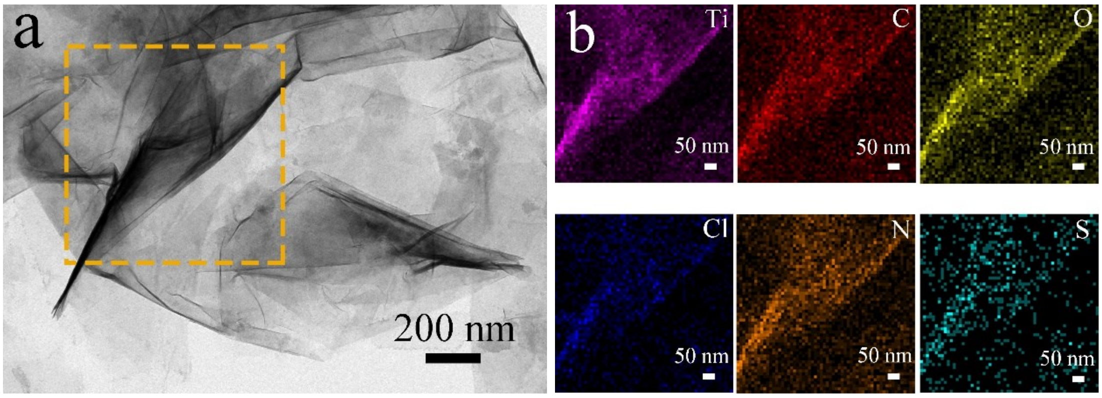

Fig. S3 (a) STEM image and (b) Elemental mapping images of Lig@$Ti_3C_2T_x$/i-PANI@$Ti_3C_2T_x$(5/5).

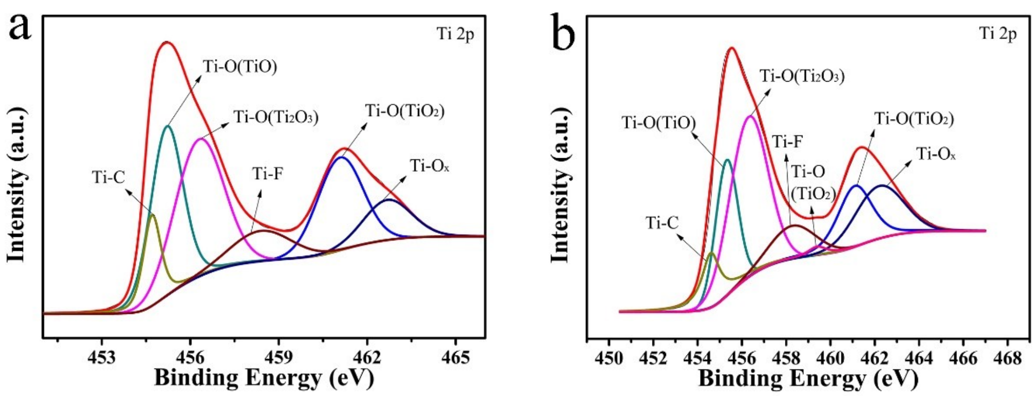

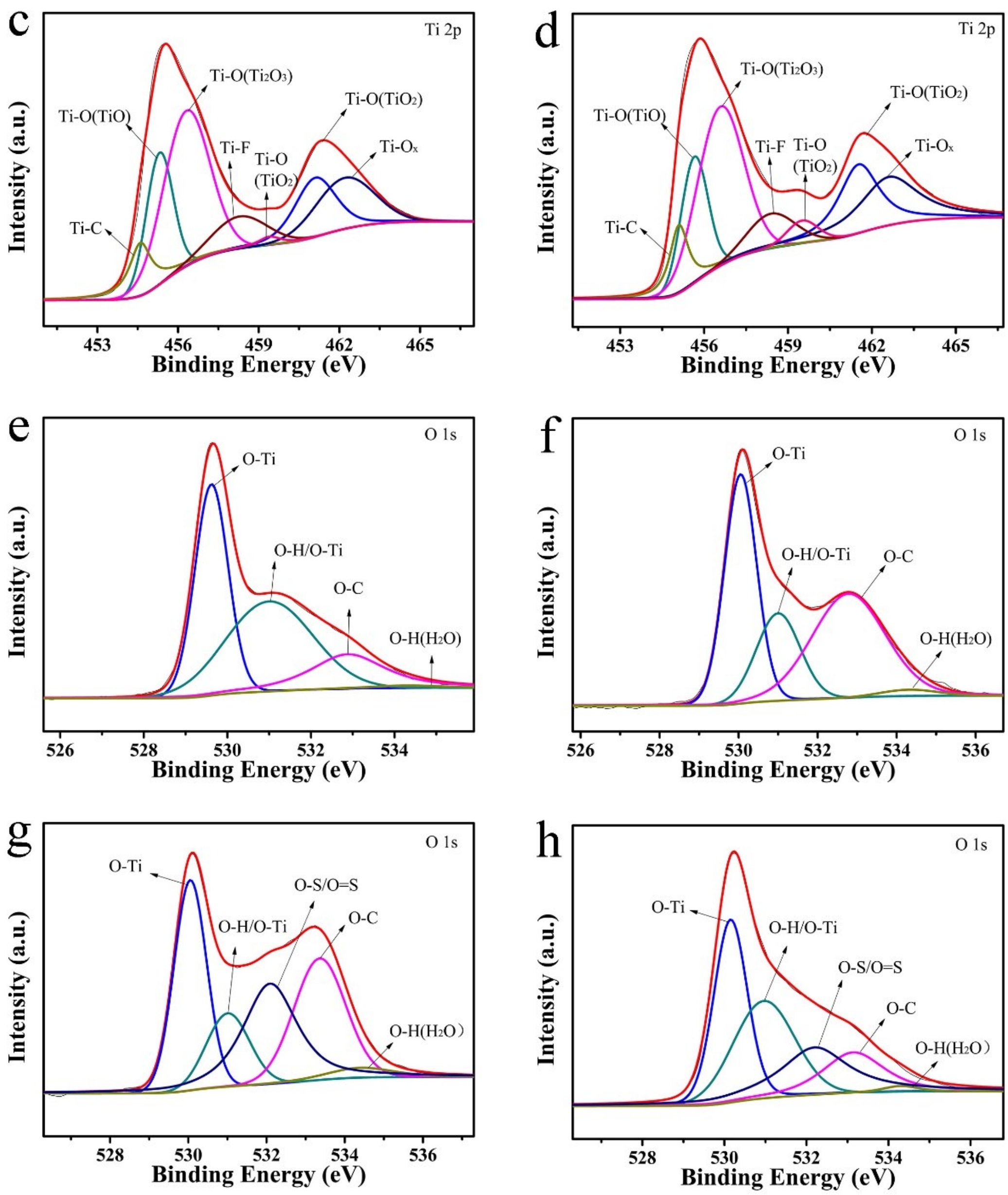

Fig. S4 The Ti 2p spectra of (a) $Ti_3C_2T_x$, (b) i-PANI@$Ti_3C_2T_x$, (c) Lig@$Ti_3C_2T_x$ and (d) Lig@$Ti_3C_2T_x$/i-PANI@$Ti_3C_2T_x$(5/5). The O 1s spectra of (e) $Ti_3C_2T_x$, (f) i-PANI@$Ti_3C_2T_x$, (g) Lig@$Ti_3C_2T_x$ and (h) Lig@$Ti_3C_2T_x$/i-PANI@$Ti_3C_2T_x$(5/5).

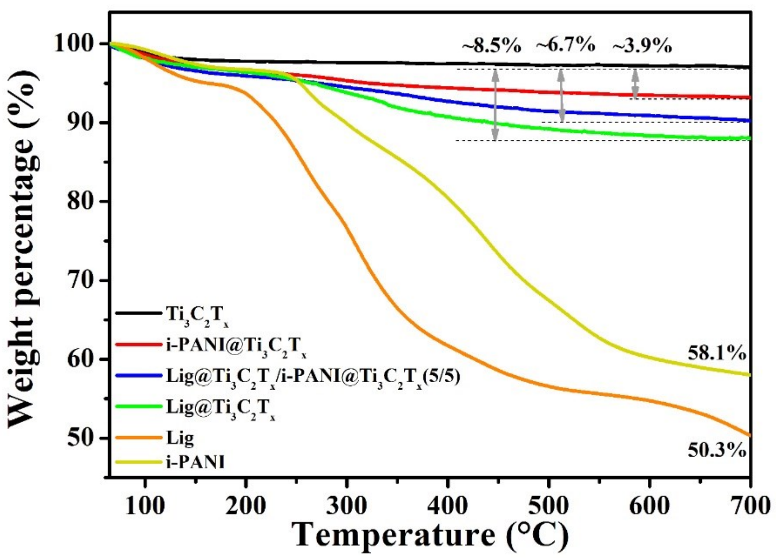

Fig. S5 The TGA curves of $Ti_3C_2T_x$, i-PANI (prepared using PPD as initiator and $FeCl_3$ as oxidant with a molar ratio of aniline:PPD=10:1 and aniline:$FeCl_3$=1:1), Lig, i-PANI@$Ti_3C_2T_x$, Lig@$Ti_3C_2T_x$ and Lig@$Ti_3C_2T_x$/i-PANI@$Ti_3C_2T_x$(5/5).

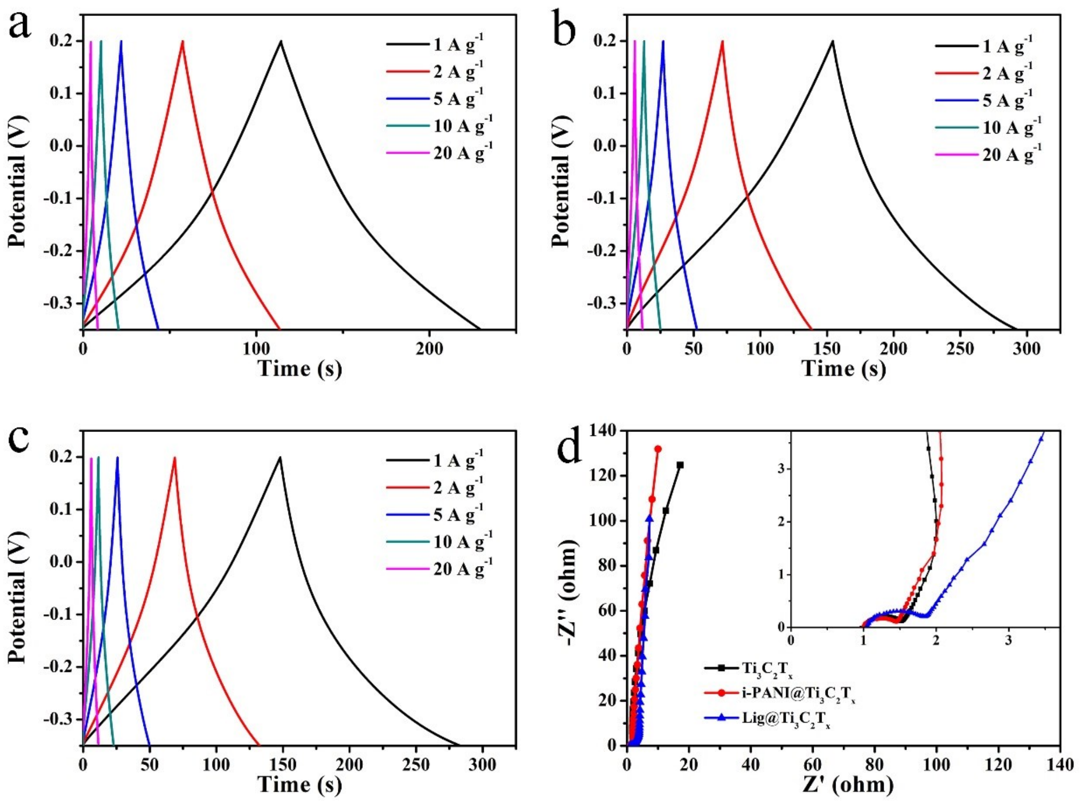

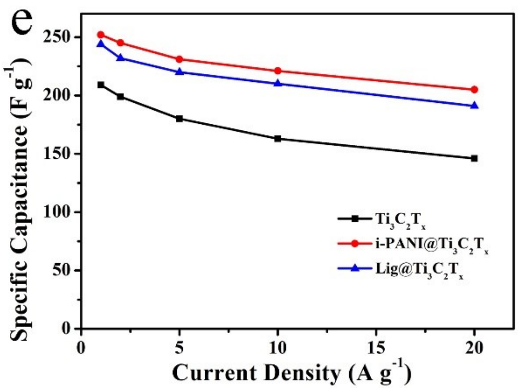

Fig. S6 Electrochemical properties of $Ti_3C_2T_x$, i-PANI@$Ti_3C_2T_x$ and Lig@$Ti_3C_2T_x$ films in three-electrode system. GCD curves of (a) $Ti_3C_2T_x$, (b) i-PANI@$Ti_3C_2T_x$ and (c) Lig@$Ti_3C_2T_x$ films in a current density range of 1 to 20 A g^{-1}, (d) Nyquist plots in a frequency range of 100 kHz to 0.01 Hz and (e) Specific capacitance at various current densities.

The electrochemical performance of i-PANI@$Ti_3C_2T_x$ film in ASSSs with different mass ratio of aniline to $Ti_3C_2T_x$ is shown in Fig. S4. The introduction of i-PANI into $Ti_3C_2T_x$ largely enhances the specific capacitance of i-PANI@$Ti_3C_2T_x$ composite films, attributed to the spacer effect and pseudocapacitance contribution of i-PANI. With increasing the mass ratio of i-PANI to $Ti_3C_2T_x$, the specific capacitance of i-PANI@$Ti_3C_2T_x$ composite films increases. While excessive amount of i-PANI may decrease the electrochemical-active surface of $Ti_3C_2T_x$, leading to decreased specific capacitance. Therefore, the most appropriate mass ratio of aniline to $Ti_3C_2T_x$ is 2:1 (aniline:PPD = 10:1).

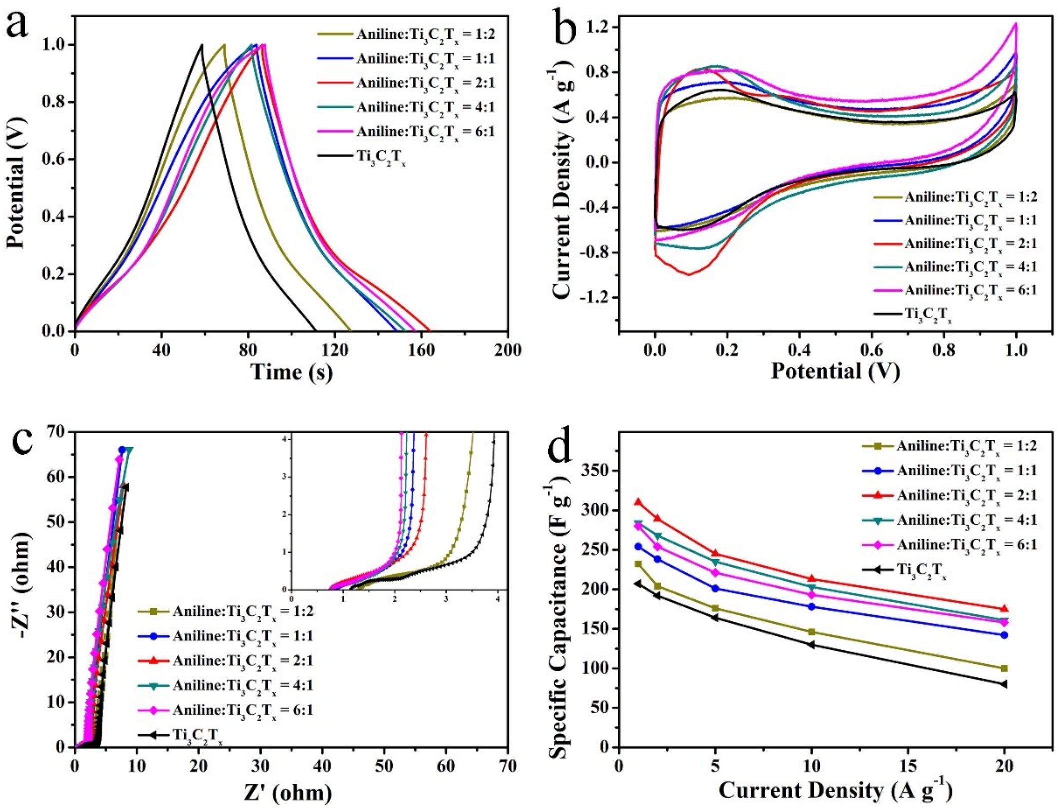

Fig. S7 Electrochemical properties of i-PANI@$Ti_3C_2T_x$ assembled ASSSs with different mass ratio of aniline to $Ti_3C_2T_x$. (a) GCD curves at a current density of 1 A g^{-1}, (b) CV curves at a scan rate of 5 mV s^{-1}, (c) Nyquist plots in a frequency range of 100 kHz to 0.01 Hz, (d) Specific capacitance of i-PANI@$Ti_3C_2T_x$ at various current densities

The influence of PPD is also investigated. The specific capacitance and rate capability of i-PANI@$Ti_3C_2T_x$ are superior to that of PANI@$Ti_3C_2T_x$ (Fig. S5). The PPD initiator may reduce oxidation potential of polymerization and adjust the structure of PANI (increasing the content of quinone), resulting in a higher rate and degree of polymerization. Therefore, the introduction of PPD can improve the electrochemical performance of i-PANI@$Ti_3C_2T_x$.

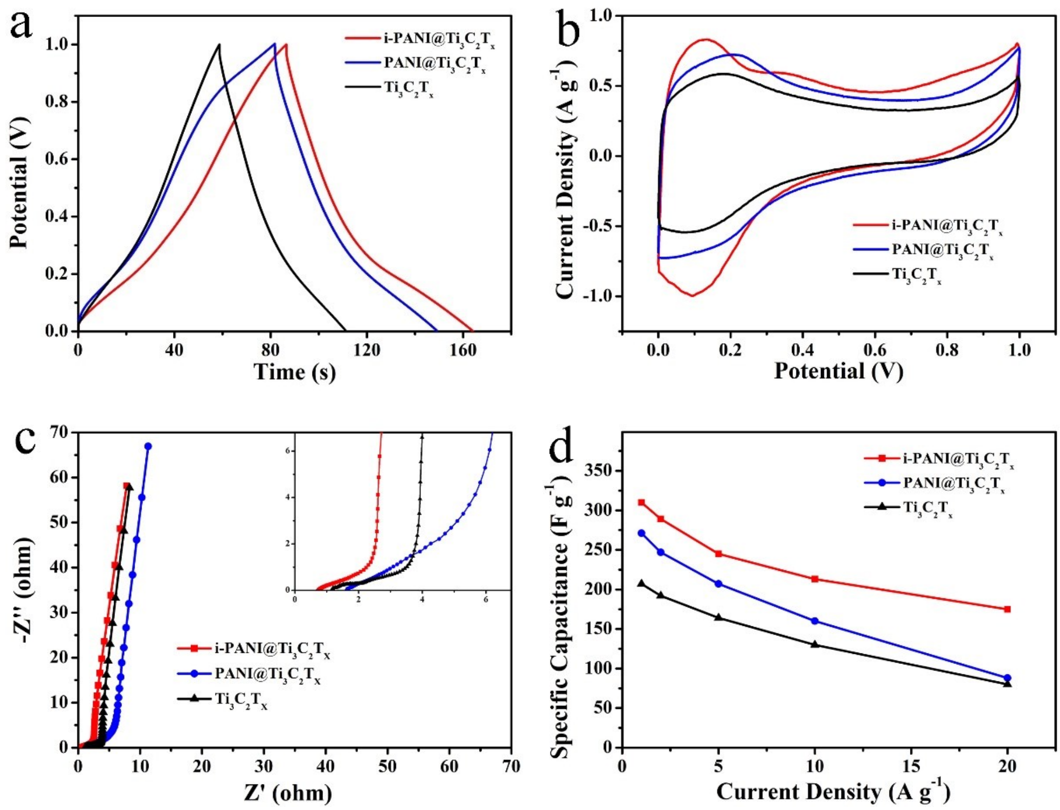

Fig. S8 Electrochemical properties of $Ti_3C_2T_x$, PANI@$Ti_3C_2T_x$ and i-PANI@$Ti_3C_2T_x$ assembled ASSSs (aniline:$Ti_3C_2T_x$ = 2:1, aniline:PPD = 10:1) film. (a) GCD curves at a current density of 1 A g^{-1}, (b) CV curves at a scan rate of 5 mV s^{-1}, (c) Nyquist plots of the samples in a frequency range of 100 kHz to 0.01 Hz, (d) Specific capacitance at various current densities.

The electrochemical performance of Lig@$Ti_3C_2T_x$ assembled ASSSs with different mass ratio of Lig to $Ti_3C_2T_x$ is shown in Fig. S6. The optimized mass ratio of Lig to $Ti_3C_2T_x$ is 2:1. Lig can effectively enhance the capacitance through redox reaction and promote the ion transfer by increasing the interlayer space. While a further increase of Lig would lead to the dramatic decrease of specific capacitance and rate capability. It is suggested that the insulative nature of Lig and the MXene sheets wrapped by excessive Lig would lead to a deterioration of layer structure and decrease of active sites.

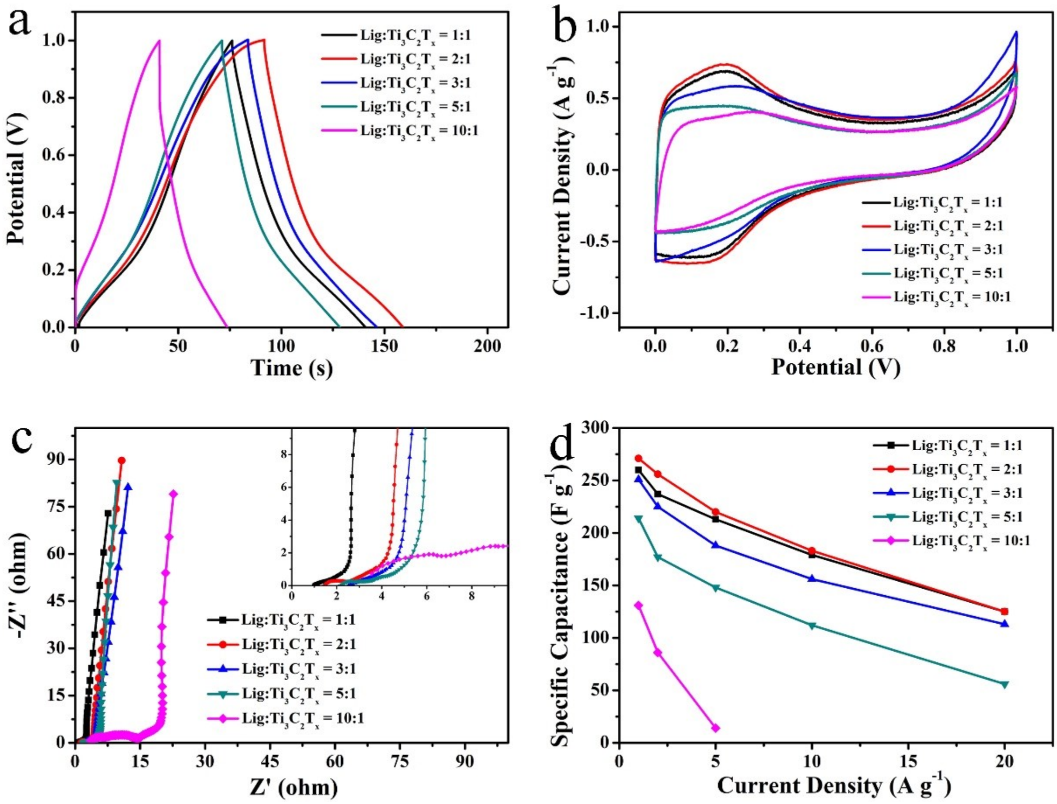

Fig. S9 Electrochemical properties of Lig@$Ti_3C_2T_x$ assembled ASSSs with different mass ration of Lig to $Ti_3C_2T_x$. (a) GCD curves at a current density of 1 A g^{-1}, (b) CV curves at a scan rate of 5 mV s^{-1}, (c) Nyquist plots in a frequency range of 100 kHz to 0.01 Hz, (d) Specific capacitance at various current densities.

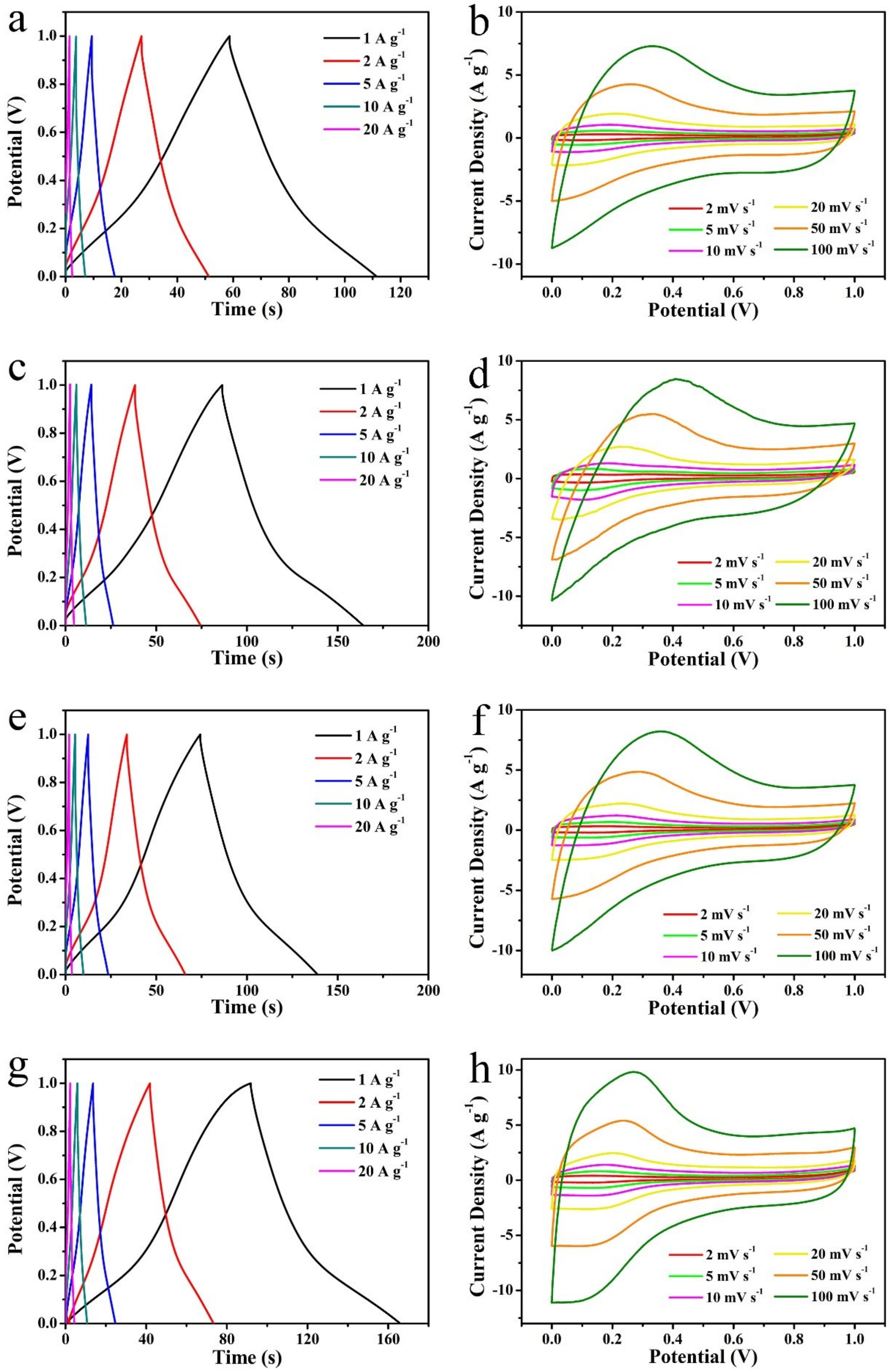

Fig. S10 Electrochemical properties of ASSSs. GCD curves of (a) $Ti_3C_2T_x$, (c) Lig@$Ti_3C_2T_x$, (e) i-PANI@$Ti_3C_2T_x$ and (g) Lig@$Ti_3C_2T_x$/i-PANI@$Ti_3C_2T_x$(5/5) films in a current density range of 1 to 20 A g^{-1} and CV curves of (b) $Ti_3C_2T_x$, (d) Lig@$Ti_3C_2T_x$, (f) i-PANI@$Ti_3C_2T_x$ and (h) Lig@$Ti_3C_2T_x$/i-PANI@$Ti_3C_2T_x$(5/5) films at scan rates ranging from 2 to 100 mV s^{-1}.

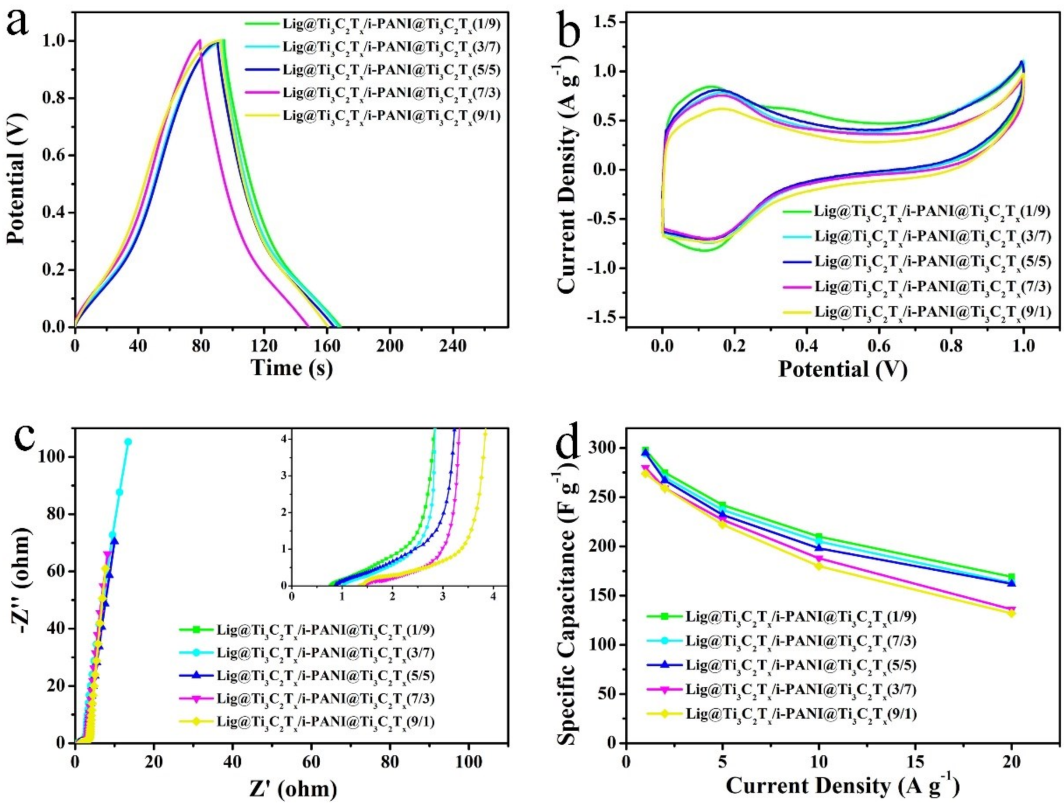

Fig. S11 Electrochemical properties of Lig@$Ti_3C_2T_x$/i-PANI@$Ti_3C_2T_x$ assembled ASSSs with different mass ratio of Lig@$Ti_3C_2T_x$ to i-PANI@$Ti_3C_2T_x$. (a) CV curves at a scan rate of 5 mV s^{-1}, (b) GCD curves at a current density of 1 A g^{-1}, (c) Nyquist plots of the samples in a frequency range of 100 kHz to 0.01 Hz and (d) Specific capacitance in various current densities.

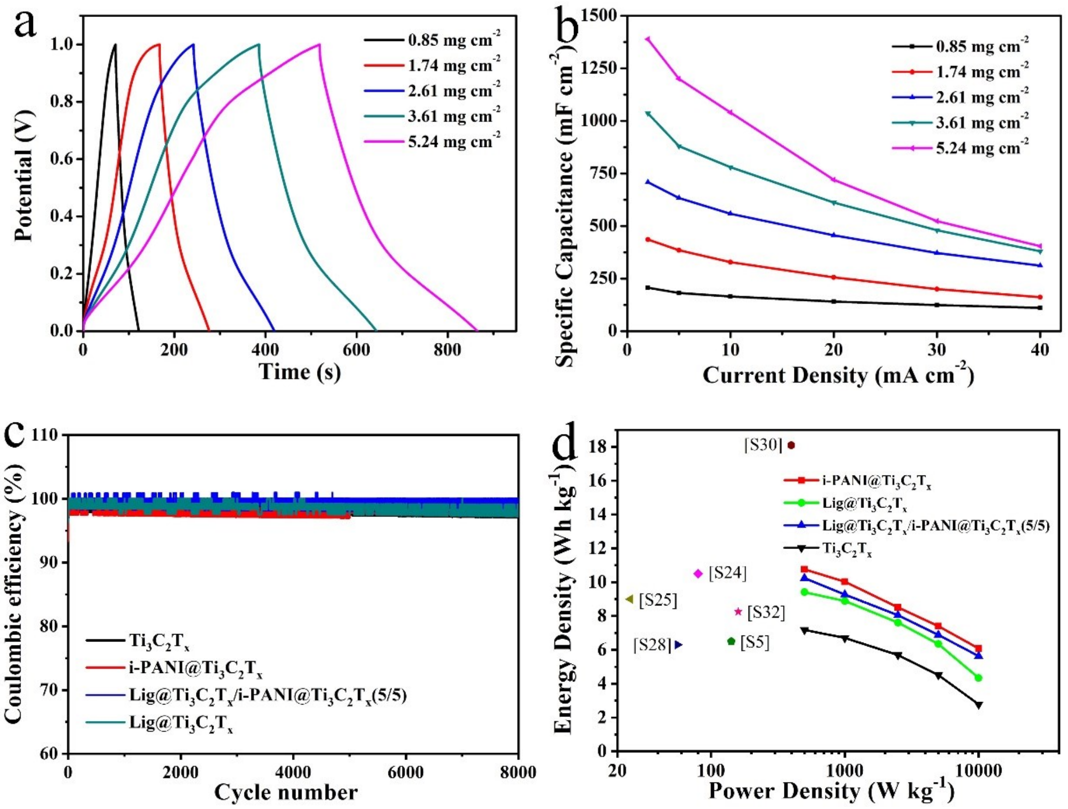

Fig. S12 Electrochemical properties of ASSSs. (a) GCD curves at a current density of 2 mA cm^{-2} and (b) areal capacitance (current density ranging from 2 to 40 mA cm^{-2}) of Lig@$Ti_3C_2T_x$/i-PANI@$Ti_3C_2T_x$(5/5) electrodes with different mass-loadings. (c) Columbic efficiency during 8000 cycles of cycling test at a current density of 10 A g^{-1}. (d) Ragone plot of energy density comparing to those reported in the literature.

Table S1. The tensile strength of some composites.

Composite films	Tensile strength (MPa)	Ref.
$Ti_3C_2T_x$ (90 wt%)/PVA film	30	S1

$Ti_3C_2T_x$ (80 wt%)/PVA film	25	S1
$Ti_3C_2T_x$/rGO-90 film	12.9	S2
$Ti_3C_2T_x$/rGO-70 film	12.3	S2
CNTs (3 mg)/$Ti_3C_2T_x$ (30 mg)/CNFs (8 mg) composite paper	98	S3
The MWCNT/$Ti_3C_2T_x$/PCL composite membrane	3	S4
$Ti_3C_2T_x$/PEDOT:PSS (mass ratios of 7:3) fibers	58.1	S5
PPy/RGO/CNT/bacterial cellulose film	57.7	S6
$Ti_3C_2T_x$/BC (mass ratios of 0.75:1) film	70	S7
i-PANI@$Ti_3C_2T_x$ film	33.2	This work
Lig@$Ti_3C_2T_x$ film	75.4	This work
Lig@$Ti_3C_2T_x$/i-PANI@$Ti_3C_2T_x$(5/5) film	53.7	This work

Table S2. The thermal diffusion coefficient, specific heat capacity, density and thermal conductivity of $Ti_3C_2T_x$, Lig@$Ti_3C_2T_x$, i-PANI@$Ti_3C_2T_x$, and Lig@$Ti_3C_2T_x$/i-PANI@$Ti_3C_2T_x$(5/5) at 25 °C.

	MXene	**Lig@$Ti_3C_2T_x$**	**i-PANI@$Ti_3C_2T_x$**	**Lig@$Ti_3C_2T_x$/i-PANI@$Ti_3C_2T_x$(5/5)**
Thermal diffusion coefficient (mm^2 s^{-1})	0.47	0.42	0.32	0.33

Specific heat capacity (J g^{-1} °C^{-1})	1.182	1.265	1.112	1.283
Density (g cm^{-3})	3.21	3.01	2.81	2.98
Thermal conductivity (W m^{-1} k^{-1})	1.78	1.60	1.01	1.26

Table S3. The through-plane thermal conductivity of some composite films.

Composites film	Through-plane thermal conductivity (W m^{-1} K^{-1})	Ref.
hBN (hydroxylated boron nitride nanosheets)@PANI	2.1	S8
rGO-cellulose nanocryst-als	4.596	S9
BN (boron nitride)/PDDA(poly(diallyl dimethyl ammonium chloride)	1.0	S10
Silicon rubber/graphene nanoplatelets/BN	0.80	S11
DOPO-g-GO (DOPO: 9, 10-dihydro-9-oxa-10-phosphaphenan-threne-10-oxide)	1.28	S12
30%-GO@PANI	0.42	S13
rGO-CNT	0.164	S14
15%-RGO@PANI	0.6	S15
hBN/polymethyl-vinyl siloxane rubber	1.11	S16

rGO-CNT	0.061	S17
PANI/graphene	19 μW m^{-1} K^{-2}	S18
50%-RGO/CNF	0.13	S19
PI (polyimide)/GO	0.32	S20
HDPE (high density polyethylene)/BN/MWCNTs/graphite	1.45	S21
PI/SiC/GO	0.577	S22
$Ti_3C_2T_x$/PVDF film	0.767	S23
i-PANI@$Ti_3C_2T_x$	1.01	This work
Lig@$Ti_3C_2T_x$	1.60	This work
Lig@$Ti_3C_2T_x$/i-PANI@$Ti_3C_2T_x$(5/5)	1.26	This work

Table S4. The capacitance of some supercapacitor electrodes.

Electrode material	Electrolyte	Specific capacitance		Ref.
$Ti_3C_2T_x$/rGO-5 wt% film	3 M H_2SO_4	80.3 F g^{-1} at 2 mV s^{-1}	two electrode system	S24
MnO_x-$Ti_3C_2T_x$ film	1 M Li_2SO_4	602.0 F cm^{-3} at 2 mV s^{-1}	two electrode system	S25
Nitrogen doped reduced graphene oxide foams (NrGFs)	6 M KOH	260 F g^{-1} at 0.1 A g^{-1}	two electrode system	S26
$Ti_3C_2T_x$/CuS composites//$Ti_3C_2T_x$ MXene	1 M KOH	49.3 F g^{-1} at 1 A g^{-1}	two electrode system	S27
$Ti_3C_2T_x$/ PEDOT:PSS //rGO film	1 M H_2SO_4	117 F cm^{-3} at 1.5 mA cm^{-2}	asymmetric, two electrode system	S29
d-$Ti_3C_2T_x$/Ni foam//b-$Ti_3C_2T_x$ film	6M KOH	51.1 F g^{-1} at 0.5 A g^{-1}	asymmetric, two electrode system	S30
N–$Ti_3C_2T_x$-300 film	3 M H_2SO_4	~150 F g^{-1} at 2mV s^{-1} 295 F cm^{-3} at 2mV s^{-1}	two electrode system	S31
Active carbon/Co_3O_4-	6M KOH	55 F g^{-1}	asymmetric,	S32

doped 3D $Ti_3C_2T_x$/rGO hybrid film		at 0.5 A g^{-1}	two electrode system	
d-$Ti_3C_2T_x$ film under 40 MPa	1 M $EMIMBF_4$/AN	244.5 F cm^{-3} at 2 mV s^{-1}	two electrode system	S33
$Ti_3C_2T_x$/MnO_2 nano wires film	PVA/LiCl gel	1025 F cm^{-3} at 1 A cm^{-3}	flexible SCs device	S34
MnO_2/$Ti_3C_2T_x$ film	PVA/H_2SO_4 gel	130.5 F g^{-1} at 0.2 A g^{-1}	flexible SCs device	S35
Metal porphyrin frameworks/$Ti_3C_2T_x$ hybrid film	PVA/H_2SO_4 gel	408 mF cm^{-2} at 0.5 mA cm^{-2}	flexible SCs device	S36
$Ti_3C_2T_x$/CNT fibers	PVA/LiCl gel	22.7 F cm^{-3} at 0.1 A cm^{-3}	solid-state fibriform SCs	S37
$Ti_3C_2T_x$ film	1 M Et_4NBF_4 /ACN	54 F g^{-1} (220 F cm^{-3}) at 2 mV s^{-1}	organic electrolyte asymmetric device	S38
$Ti_3C_2T_x$/rGO//$Ti_3C_2T_x$ film	1 M Et_4NBF_4 /ACN	48 F g^{-1} (78 F cm^{-3}) at 2 mV s^{-1}	organic electrolyte asymmetric device	S38
N-doping cotton-derived carbon frameworks/graphene aerogel	PVA/KOH gel	~200 F g^{-1} at 0.1 A g^{-1}	all-solid-state SCs	S39
PANI/orderly nanotube array film	PVA/H_2SO_4 gel	237.5 mF cm^{-2} at 10 mV s^{-1}	flexible all-solid-state SCs	S40
Fe_3O_4/carbon nanotube/polyaniline ternary film	PVA/H_2SO_4 gel	201 F g^{-1} at 20 mV s^{-1}	all-solid-state SCs	S41
CNT/PANI composite film	PAAm/LiCl hydrogel	99.3 F cm^{-3} at 0.1 mA cm^{-3}	all-solid-state SCs	S42
$Ti_3C_2T_x$	PVA/H_2SO_4 gel	27.29 mF cm^{-2} at 2 mV s^{-1}	Micro-SCs	S43
$Ti_3C_2T_x$/rGO	PVA/H_2SO_4 gel	80 F cm^{-3} at 2 mV s^{-1}	Micro-SCs	S44
Ascorbate/$Ti_3C_2T_x$	PVA/H_2SO_4 gel	720.7 F cm^{-3} at 1 A g^{-1}	Micro-SCs	S45
Hierarchical $Ti_3C_2T_x$	PVA/H_3PO_4 gel	485 F cm^{-3} at 1 A cm^{-3}	all-solid-state SCs	S46
PEDOT:PSS/$Ti_3C_2T_x$ (PEDOT:poly(3,4-ethylenedioxythiophene)	PVA/H_2SO_4 gel	361.4 F cm^{-3} at 2 mV s^{-1}	fiber-shaped SCs	S5

(PPS: poly(styrenesulfonate))				
$Ti_3C_2T_x$/rGO-90 fibers	PVA/H_3PO_4 gel	586.4 F cm^{-3} at 10 mV s^{-1}	fiber based all-solid-state symmetric SCs	S2
$Ti_3C_2T_x$/GO fibers	PVA/H_2SO_4 gel	256 F cm^{-3} at 0.1 A cm^{-3}	fiber SCs device	S47
$Ti_3C_2T_x$ film	PVA/H_2SO_4 gel	183 F cm^{-3} at 0.25 mA cm^{-2}	flexible solid-state Micro-SCs	S48
Electrochemically exfoliated graphene/ $Ti_3C_2T_x$ film	PVA/H_3PO_4 gel	216 F cm^{-3} at 0.1 A cm^{-3}	flexible all-solid-state SCs	S49
PANI/bacterial cellulose//$Ti_3C_2T_x$/bacterial cellulose	PVA/H_2SO_4 gel	585 mF cm^{-2} at 3 mA cm^{-21}	flexible all-solid-state SCs	S50
RuO_2//$Ti_3C_2T_x$	PVA/H_3PO_4 gel	60 mF cm^{-2} at 5 mV s^{-1}	all-solid-state SCs	S51
PANI@ANF film	PVA/H_2SO_4 gel	138 F g^{-1} at 0.5 A g^{-1}	all-solid-state SCs	S52
i-PANI@$Ti_3C_2T_x$ film	PVA/H_2SO_4 gel	310 F g^{-1} (1001 F cm^{-3}) at 1 A g^{-1}	flexible all-solid-state SCs	This work
Lig@$Ti_3C_2T_x$ film	PVA/H_2SO_4 gel	271 F g^{-1} (881 F cm^{-3}) at 1 A g^{-1}	flexible all-solid-state SCs	This work
Lig@$Ti_3C_2T_x$/i-PANI@$Ti_3C_2T_x$(5/5) film	PVA/H_2SO_4 gel	295 F g^{-1} (959 F cm^{-3}) at 1 A g^{-1}	flexible all-solid-state SCs	This work

Table S5. The comparison of energy density of previously reported supercapacitor and the as-prepared flexible ASSSs.

Electrode material	**Electrolyte**	**Gravimetric power density (Wh kg^{-1})**	**Volume power density (Wh L^{-3})**		**Ref.**
$Ti_3C_2T_x$/rGO-5 wt% film	3 M H_2SO_4	10.5 at 80.3 W kg^{-1}	32.6 at 200 W L^{-1}	two electrode system	S24
MnO_x-$Ti_3C_2T_x$ film	1 M Li_2SO_4	/	13.64 at 2 mV s^{-1}	two electrode system	S25

Nitrogen doped reduced graphene oxide foams (NrGFs)	6 M KOH	9 at 25 W kg^{-1}	/	two electrode system	S26
$Ti_3C_2T_x$/CuS composites//$Ti_3C_2T_x$ MXene	1 M KOH	15.4 at 750.2 W kg^{-1}	/	asymmetric, two electrode system	S27
$Fe(OH)_3$/$Ti_3C_2T_x$ film	3 M H_2SO_4	6.3 at 56 W kg^{-1}	20.7 at 184.8 W L^{-1}	two electrode system	S28
$Ti_3C_2T_x$/PEDOT:PSS//rGO film	1 M H_2SO_4	/	23 at 7659 W L^{-1}	asymmetric, two electrode system	S29
d-$Ti_3C_2T_x$/Ni foam//b-$Ti_3C_2T_x$ film	6M KOH	18.1 at 397.8 W kg^{-1}	/	asymmetric, two electrode system	S30
N–$Ti_3C_2T_x$-300 film	3 M H_2SO_4	/	21.0 at 151.3 W L^{-1}	two electrode system	S31
Active carbon/Co_3O_4-doped 3D $Ti_3C_2T_x$/rGO hybrid film	6M KOH	8.25 at 159.94 W kg^{-1}	/	two electrode system	S32
d-$Ti_3C_2T_x$ film under 40 MPa	1 M $EMIMBF_4$/AN	/	41 at 108 W L^{-1} (27 at 500 W L^{-1})	two electrode system	S33
$Ti_3C_2T_x$/MnO_2 nano wires film	PVA/LiCl gel	/	56.94 at 500 W L^{-1}	flexible SCs device	S34
MnO_2/$Ti_3C_2T_x$ film	PVA/H_2SO_4 gel	/	0.7 μWh cm^{-2} at 80.0 μW cm^{-2}	flexible SCs device	S35
Metal porphyrin frameworks/$Ti_3C_2T_x$ hybrid film	PVA/H_2SO_4 gel	/	20.4 μW h cm^{-2} at 152.2 μW cm^{-2}	flexible SCs device	S36
$Ti_3C_2T_x$/CNT fibers	PVA/LiCl gel	/	2.55 at 45.9 W L^{-1}	solid-state fibriform SCs	S37
$Ti_3C_2T_x$/MWCNT film	1 M Et_4NBF_4 /ACN	3 at 60 W kg^{-1}	/	organic electrolyte symmetric device	S38
$Ti_3C_2T_x$/rGO//$Ti_3C_2T_x$ film	1 M Et_4NBF_4 /ACN	8 at 55 W kg^{-1}	15 at 90 W L^{-1}	organic electrolyte	S38

				asymmetric device	
N-doping cotton-derived carbon frameworks/graphene aerogel film	PVA/KOH gel	20 at 4000 W kg^{-1}	/	all-solid-state SCs	S39
PANI/orderly nanotube array film	PVA/H_2SO_4 gel	/	24.31 at 2.74 W L^{-1}	flexible all-solid-state SCs	S40
Fe_3O_4/carbon nanotube/polyaniline ternary film	PVA/H_2SO_4 gel	28.0 at 5.3 kW kg^{-1}	/	all-solid-state SCs	S41
CNT/PANI composite film	PAAm/LiCl hydrogel	/	8.8 at 370 W L^{-1}	all-solid-state SCs	S42
$Ti_3C_2T_x$	PVA/H_2SO_4 gel	/	6.1 at 200 W L^{-1}	Micro-SCs	S43
$Ti_3C_2T_x$/rGO	PVA/H_2SO_4 gel	/	8.6 at 200 W L^{-1}	Micro-SCs	S44
Ascorbate/$Ti_3C_2T_x$	PVA/H_2SO_4 gel	/	100.2 at 1900 W L^{-1}	Micro-SCs	S45
Hierarchical $Ti_3C_2T_x$	PVA/H_3PO_4 gel	/	9.6 at 2800 W L^{-1}	all-solid-state SCs	S46
PEDOT:PSS/$Ti_3C_2T_x$	PVA/H_2SO_4 gel	6.49 at 142.16 W L^{-1}	7.13 at 142.16 W L^{-1}	fiber-shaped SCs	S5
$Ti_3C_2T_x$/rGO-90 fibers	PVA/H_3PO_4 gel	/	13.03 at 590 W L^{-1}	fiber based all-solid-state symmetric SCs	S2
$Ti_3C_2T_x$/GO fibers	PVA/H_2SO_4 gel	/	5.1 at 200 W L^{-1}	fiber SCs device	S47
$Ti_3C_2T_x$ film	PVA/H_2SO_4 gel	/	12.4 at 87.5 W cm^{-2}	flexible solid-state Micro-SCs	S48
Electrochemically exfoliated graphene/ $Ti_3C_2T_x$ film	PVA/H_3PO_4 gel	/	3.4 at 200 W L^{-1}	flexible all-solid-state SCs	S49
PANI/bacterial cellulose//$Ti_3C_2T_x$/bacterial cellulose	PVA/H_2SO_4 gel	/	159 µWh cm^{-2} at 34.4 mW cm^{-2}	flexible all-solid-state SCs	S50
RuO_2//$Ti_3C_2T_x$	PVA/H_3PO_4 gel	/	37 µW h cm^{-2} at 40 mW cm^{-2}	solid-state device	S51
NiCoS/CC//AC	2 M KOH	40 at 379 W	/	asymmetri	S53

		kg^{-1}		c, two electrode system	
i-PANI@$Ti_3C_2T_x$ film	PVA/H_2SO_4 gel	10.76 at 500 W kg^{-1}	34.8 at 1615 W L^{-1}	flexible all-solid-state SCs	This work
Lig@$Ti_3C_2T_x$ film	PVA/H_2SO_4 gel	9.41 at 500 W kg^{-1}	30.6 at 1625 W L^{-1}	flexible all-solid-state SCs	This work
Lig@$Ti_3C_2T_x$/i-PANI@$Ti_3C_2T_x$(5/5) film	PVA/H_2SO_4 gel	10.24 at 500 W kg^{-1}	33.3 at 1625 W L^{-1}	flexible all-solid-state SCs	This work

References

1 Z. Ling, C. E. Ren, M.-Q. Zhao, J. Yang, J. M. Giammarco, J. Qiu, M. W. Barsoum and Y. Gogotsi, *Proc. Natl. Acad. Sci.*, 2014, **111**, 16676-16681.

2 Q. Yang, Z. Xu, B. Fang, T. Huang, S. Cai, H. Chen, Y. Liu, K. Gopalsamy, W. Gao and C. Gao, *J. Mater. Chem. A*, 2017, **5**, 22113-22119.

3 W. Cao, C. Ma, S. Tan, M. Ma, P. Wan and F. Chen, *Nano-Micro Lett.*, 2019, **11**, 72.

4 Z. Zhou, W. Panatdasirisuk, T. S. Mathis, B. Anasori, C. Lu, X. Zhang, Z. Liao, Y. Gogotsi and S. Yang, *Nanoscale*, 2018, **10**, 6005-6013.

5 J. Zhang, S. Seyedin, S. Qin, Z. Wang, S. Moradi, F. Yang, P. A. Lynch, W. Yang, J. Liu, X. Wang and J. M. Razal, *Small*, 2019, **15**, 1804732.

6 Y. Bai, R. Liu, E. Li, X. Li, Y. Liu and G. Yuan, *J. Alloys Compd.*, 2019, **777**, 524-530.

7 S. Jiao, A. Zhou, M. Wu and H. Hu, *Adv. Sci.*, 2019, **6**, 1900529.

8 Y. Bai, W. Han, C. Ge, R. Liu, R. Zhang, L. Wang and X. Zhang, *Macromol. Mater. Eng.*, 2019, **304**, 1900442.

9 X. Meng, H. Pan, C. Zhu, Z. Chen, T. Lu, D. Xu, Y. Li and S. Zhu, *ACS Appl. Mater. Interfaces*, 2018, **10**, 22611-22622.

10 Y. Wu, Y. Xue, S. Qin, D. Liu, X. Wang, X. Hu, J. Li, X. Wang, Y. Bando, D. Golberg, Y. Chen, Y. Gogotsi and W. Lei, *ACS Appl. Mater. Interfaces*, 2017, **9**, 43163-43170.

11 C.-P. Feng, S.-S. Wan, W.-C. Wu, L. Bai, R.-Y. Bao, Z.-Y. Liu, M.-B. Yang, J. Chen and W. Yang, *Compos. Sci. Technol.*, 2018, **167**, 456-462.

12 F. Luo, K. Wu, F. Xiao, X. Du and M. Lu, *Compos. Part A Appl. Sci. Manuf.*, 2019, **116**, 72-78.

13 G. Yun, S.-Y. Tang, S. Sun, D. Yuan, Q. Zhao, L. Deng, S. Yan, H. Du, M. D. Dickey and W. Li, *Nat. Commun.*, 2019, **10**, 1300.

14 H. Lu, J. Zhang, J. Luo, W. Gong, C. Li, Q. Li, K. Zhang, M. Hu and Y. Yao, *Compos. Part A Appl. Sci. Manuf.*, 2017, **102**, 1-8.

15 L. Wang, Q. Yao, H. Bi, F. Huang, Q. Wang and L. Chen, *J. Mater. Chem. A*, 2014, **2**, 11107-11113.

16 J. Gu, X. Meng, Y. Tang, Y. Li, Q. Zhuang and J. Kong, *Compos. Part A Appl. Sci. Manuf.*, 2017, **92**, 27-32.

17 T.-W. Pan, W.-S. Kuo and N.-H. Tai, *Compos. Sci. Technol.*, 2017, **151**, 44-51.

18 R. Islam, R. Chan-Yu-King, J.-F. Brun, C. Gors, A. Addad, M. Depriester, A. Hadj-Sahraoui and F. Roussel, *Nanotechnology*, 2014, **25**, 475705.

19 W. Yang, Z. Zhao, K. Wu, R. Huang, T. Liu, H. Jiang, F. Chen and Q. Fu, *J. Mater. Chem. C*, 2017, **5**, 3748-3756.

20 I.-H. Tseng, J.-C. Chang, S.-L. Huang and M.-H. Tsai, *Polym. Int.*, 2013, **62**, 827-835.

21 X. Zhang, J. Zhang, C. Li, J. Wang, L. Xia, F. Xu, X. Zhang, H. Wu and S. Guo, *Chem. Eng. J.*, 2017, **328**, 609-618.

22 W. Dai, J. Yu, Z. Liu, Y. Wang, Y. Song, J. Lyu, H. Bai, K. Nishimura and N. Jiang, *Compos. Part A Appl. Sci. Manuf.*, 2015, **76**, 73-81.

23 K. Rajavel, S. Luo, Y. Wan, X. Yu, Y. Hu, P. Zhu, R. Sun and C. Wong, *Compos. Part A Appl. Sci. Manuf.*, 2020, **129**, 105693.

24 J. Yan, C. E. Ren, K. Maleski, C. B. Hatter, B. Anasori, P. Urbankowski, A. Sarycheva and Y. Gogotsi, *Adv. Funct. Mater.*, 2017, **27**, 1701264.

25 Y. Tian, C. Yang, W. Que, X. Liu, X. Yin and L. B. Kong, *J. Power Sources*, 2017, **359**, 332-339.

26 D. Liu, Q. Li, S. Li, J. Hou and H. Zhao, *Nanoscale*, 2019, **11**, 4362-4368.

27 Z. Pan, F. Cao, X. Hu and X. Ji, *J. Mater. Chem. A*, 2019, **7**, 8984-8992.

28 Z. Fan, Y. Wang, Z. Xie, X. Xu, Y. Yuan, Z. Cheng and Y. Liu, *Nanoscale*, 2018, **10**, 9642-9652.

29 L. Li, N. Zhang, M. Zhang, X. Zhang and Z. Zhang, *Dalton Trans.*, 2019, **48**, 1747-1756.

30 J. Guo, Y. Zhao, A. Liu and T. Ma, *Electrochim. Acta*, 2019, **305**, 164-174.

31 Y. Tian, W. Que, Y. Luo, C. Yang, X. Yin and L. B. Kong, *J. Mater. Chem. A*, 2019, **7**, 5416-5425.

32 R. Liu, A. Zhang, J. Tang, J. Tian, W. Huang, J. Cai, C. Barrow, W. Yang and J.

Liu, *Chem. Eur. J.*, 2019, **25**, 5547-5554.

33 C. Yang, Y. Tang, Y. Tian, Y. Luo, Y. He, X. Yin and W. Que, *Adv. Funct. Mater.*, 2018, **28**, 1705487.

34 J. Zhou, J. Yu, L. Shi, Z. Wang, H. Liu, B. Yang, C. Li, C. Zhu and J. Xu, *Small*, 2018, **14**, 1803786.

35 H. Jiang, Z. Wang, Q. Yang, M. Hanif, Z. Wang, L. Dong and M. Dong, *Electrochim. Acta*, 2018, **290**, 695-703.

36 W. Zhao, J. Peng, W. Wang, B. Jin, T. Chen, S. Liu, Q. Zhao and W. Huang, *Small*, 2019, **15**, 1901351.

37 C. Yu, Y. Gong, R. Chen, M. Zhang, J. Zhou, J. An, F. Lv, S. Guo and G. Sun, *Small*, 2018, **14**, 1801203.

38 A. M. Navarro-Suárez, K. L. Van Aken, T. Mathis, T. Makaryan, J. Yan, J. Carretero-González, T. Rojo and Y. Gogotsi, *Electrochim. Acta*, 2018, **259**, 752-761.

39 Y.-M. Fan, W.-L. Song, X. Li and L.-Z. Fan, *Carbon*, 2017, **111**, 658-666.

40 H. Li, J. Song, L. Wang, X. Feng, R. Liu, W. Zeng, Z. Huang, Y. Ma and L. Wang, *Nanoscale*, 2017, **9**, 193-200.

41 J. Li, W. Lu, Y. Yan and T.-W. Chou, *J. Mater. Chem. A*, 2017, **5**, 11271-11277.

42 H. Li, T. Lv, N. Li, Y. Yao, K. Liu and T. Chen, *Nanoscale*, 2017, **9**, 18474-18481.

43 H. Hu and T. Hua, *J. Mater. Chem. A*, 2017, **5**, 19639-19648.

44 C. Couly, M. Alhabeb, K. L. Van Aken, N. Kurra, L. Gomes, A. M. Navarro-

Suárez, B. Anasori, H. N. Alshareef and Y. Gogotsi, *Adv. Electron. Mater.*, 2018, **4**, 1700339.

45 C.-W. Wu, B. Unnikrishnan, I.-W. Peter Chen, S. G. Harroun, H.-T. Chang and C.-C. Huang, *Energy Storage Mater.*, 2020, **25**, 563-571.

46 Q. Pan, C. Duan, H. Liu, M. Li, Z. Zhao, D. Zhao, Y. Duan, Y. Chen and Y. Wang, *ACS Appl. Energy Mater.*, 2019, **2**, 6834-6840.

47 S. Seyedin, E. R. S. Yanza and J. M. Razal, *J. Mater. Chem. A*, 2017, **5**, 24076-24082.

48 H. Huang, H. Su, H. Zhang, L. Xu, X. Chu, C. Hu, H. Liu, N. Chen, F. Liu, W. Deng, B. Gu, H. Zhang and W. Yang, *Adv. Electron. Mater.*, 2018, **4**, 1800179.

49 H. Li, Y. Hou, F. Wang, M. R. Lohe, X. Zhuang, L. Niu and X. Feng, *Adv. Energy Mater.*, 2017, **7**, 1601847.

50 Y. Wang, X. Wang, X. Li, Y. Bai, H. Xiao, Y. Liu, R. Liu and G. Yuan, *Adv. Funct. Mater.*, 2019, **29**, 1900326.

51 Q. Jiang, N. Kurra, M. Alhabeb, Y. Gogotsi and H. N. Alshareef, *Adv. Energy Mater.*, 2018, **8**, 1703043.

52 Q. Yin, H. Jia, A. Mohamed, Q. Ji, L. Hong. *Nanoscale*, 2020, **12**, 5507-5520.

53 T. Liu, J. Liu, L. Zhang, B. Cheng, J. Yu. *J. Mater. Sci. Technol.*, 2020, **47**, 113-121.